"This article is dedicated to Prof. Huen Lee on the occasion of his retirement from KAIST"

Generation of micro- and nano-bubble distributions in water via dissociation of gas hydrates

Tsutomu Uchida†, Kenji Yamazaki, and Kazutoshi Gohara

Division of Applied Physics, Faculty of Engineering, Hokkaido University

N13 W8 Kita-ku, Sapporo 060-8628, Japan

Abstract

Gas hydrate crystals have a structure in which one molecule is enclathrated in a cage of water molecules. When such a crystal dissociates in water, each enclathrated molecule, generally vapor at standard temperature and pressure, directly dissolves into the water. After the solution is supersaturated, excess gas molecules from further dissociation would start forming small bubbles called micro- and nano-bubbles (MNBs). However, it is difficult to identify such small bubbles dispersed in liquid because they are smaller than a microscope's optical resolution. To confirm the formation of MNBs after gas hydrate dissociation, we used a transmission electron microscope (TEM) to analyze freeze-fracture replicas of CH_4-hydrate dissociation solution. The TEM images indicate the existence of MNBs in the solution, with a number concentration similar to that from a commercially supplied generator. Raman spectroscopic measurements on the CH_4-hydrate dissociated solution were then done to confirm that the MNBs contain CH_4 vapor, and to estimate experimentally the inner pressure of the CH_4 MNBs. These results suggest that the dissociation of gas hydrate crystals in water is a simple, effective method to obtain MNB solution. We then discuss how such MNBs may play a key role in the memory effect of gas-hydrate reformation.

Keywords

Microbubble, Nanobubble, gas hydrate dissociation, freeze fracture replica, bubble pressure, memory effect

INTRODUCTION

Small bubbles are either microbubbles (MBs), being about one to a hundred micrometers in diameter, and nanobubbles (NBs), which are submicron. Here we use the term micro- and nano-bubbles (MNBs) to include all diameters less than several micrometers. MNBs have recently attracted considerable attention as a functional material for industrial applications, such as wastewater purification, water-quality improvement, sterilization, decolorization, and the promotion of the physiological activities of living organisms [1]. These applications are based on the unique properties of MNBs. For example, MNBs have a negligible rise speed in water [2]. The rise of a bubble in water will nearly always equal its terminal velocity V, estimated using Stoke's Law as [3]

$$V = (\rho_g - \rho_l)\, g\, d^2 / 18\, \eta, \tag{1}$$

where ρ_g and ρ_l are the densities of the particle and that of the surrounding liquid, respectively, g is the gravitational acceleration, d is the particle diameter, and η is the viscosity of the surrounding liquid. This equations predicts that V is approximately 6×10^{-9} m s^{-1} for a 100-nm diameter MNB in water at 298 K, which is 10^6 times smaller than that of a MB with d = 100 μm [4]. This estimate indicates that MNBs can stay longer at a specific area in the solution.

However, the lifetime of MNBs remains unknown. According to the Young-Laplace equation, the pressure of gas inside the bubble is

$$P_g = P_l + 4\sigma/d, \tag{2}$$

where P_g and P_l are the gas and the liquid pressure, respectively, and σ is the surface tension of water. This equation shows that smaller bubbles have larger inner pressure, and therefore they dissolve faster according to Henry's Law. For example, Ljunggren and Eriksson [5] calculated that the lifetime of an air bubble with radii between 10 and 100 nm ranges from about 1 to 100 μs. This short lifetime seems contradictory to experimental results showing that MNBs in water have physiological-activity-promoting or sterilization

effects [1, 6]. This contradiction has not been resolved because we lack the experimental techniques for observing MNBs dispersed in liquid and for measuring the pressure P_g in MNBs. While the shrinkage of MBs in water can be observed in an optical microscope, it is impossible to determine visually whether the bubble finally disappears by dissolving in the water or remains as a MNB of diameter too small to resolve with a microscope. But recently, MNBs have been observed in bulk liquids by using electron microscopy with the freeze-fracture replica technique [7-10].

Usually, the solution containing MNBs is prepared by an MB generator, in which some amount of bubbles shrink to form MNBs and remain in the solution. To obtain a solution including a significant amount of MNBs, a longer generation period is required [11]. As another method, gas hydrates are a potential generator of MNB solution due to their unique structure. Gas hydrates are crystalline solid compounds consisting of hydrogen-bonded water molecules forming cages around enclosed gas molecules. When they are dissociated in solution, the formerly enclathrated gas molecules would at first dissolve into the solution and then, after saturation is reached, form bubbles. If these bubbles are MNBs, then the dissociation method would be a simple but different way to generate MNBs.

In addition, the formation and dissociation mechanisms of hydrate crystals are important for various energy and environmental issues, such as preventing internal hydrate plugs that block gas pipelines [12], storing and transporting natural gases in the form of gas hydrates [13], and exploiting natural gases from deep-sea sediments without geohazards [14, 15]. To use gas hydrates as a functional material for industry, it is necessary to control their formation and dissociation processes. A method to accelerate gas-hydrate formation involves the use of a thermal hysteresis process called the ‘memory effect’, which is recognized as a shortening of the induction time of gas hydrate nucleation upon recrystallization after the initial crystallization. For example, Parent and Bishnoi [16] and Takeya et al. [17] show that the memory effect may occur using meltwater from gas hydrate in the methane (CH_4)/water system and the carbon dioxide (CO_2)/water system, respectively. Sloan and Koh [18] summarized the memory effect phenomena, and showed that its behavior was predicted by two previously proposed hypotheses: 1) the hydrate structure remained in solution after hydrate dissociation [16, 17], and 2) dissolved gas remained in solution after hydrate dissociation [19]. If a significant amount of MNBs including guest molecules remains longer in the dissolved solution, the second hypothesis would be important.

Molecular dynamic simulations recently predicted the formation of NBs in solution after gas hydrate

dissociation [20-23]. However, it is still difficult to directly confirm the existence of MNBs dispersed in the solution. Thus, we use here the method of imaging freeze-fracture replica via a transmission electron microscopy (TEM) to examine the solution after CH_4 hydrate dissociation. We find MNBs in the solution formed by dissociation of CH_4 hydrate. Their size distribution is similar to that obtained from a MB generator. But the size distribution of MNBs is found to depend on the storage period.To confirm that the MNB contains CH_4, Raman spectroscopic measurements were done on the solution after CH_4 hydrate dissociation. We find CH_4 molecules from the vapor phase, with a pressure P_g (according to the shift in C-H symmetric stretching (ν_1) mode) of about 7 MPa. This is the first experimental data on P_g although it is slightly lower than that expected theoretically. Then we argue that this gas-hydrate-dissolution method is a simple and effective method to obtain significant amounts of MNBs. Moreover, such MNBs are likely an important influence on the memory effect of gas hydrates.

EXPERIMENTAL METHOD AND MATERIAL

To prepare the CH_4 hydrate crystal, we combined 50 mL of distilled, deionized water (15 MΩ cm resistivity) with approximately 4.5-MPa pure CH_4 gas (99.995 vol% in purity, Hokkaido Air Water) in a high-pressure vessel equipped with a mechanical stirrer, a sheathed thermocouple (type K), and pressure gauge (Nagano Keiki Seisakusho, type KH15). The vessel was set in a temperature-controlled bath at 274.2 ± 0.2 K and the mechanical stirrer was run at about 300 rpm for several hours. After the CH_4 hydrate formation was finished, the vessel was cooled below 173.2 K, and then the vessel was opened to recover the solid sample including ice and CH_4 hydrate crystal. The hydrate fraction in the solid sample was about 0.7, which was estimated by measuring the weight and gas volume and assuming a cage occupancy of 0.93 [25]. More details of this method are in [25].

Several samples of CH_4 hydrate were then immersed into 4-mL of distilled and deionized wate at room-temperature in a silica-glass cell used for Raman spectroscopic measurements. During and after the CH_4 hydrate dissociation, a small amount of the dissociated solution (less than 3 μL) was sampled and frozen quickly by putting it on the Au-coated Cu sample holder and immersing it into a liquid nitrogen bath to preserve the MNBs in the frozen droplet. In this condition, the freezing rate exceeds 10^3 K min^{-1}. For the

subsequent freeze-fracture replica formation, we followed the procedure in [10, 26], and give only a brief description here. To reduce the formation of artifacts during the replica film formation, the frozen droplet was fractured under vacuum (10^{-4} to 10^{-5} Pa) and low temperature (about 100 K). Then we evaporated platinum and carbon (JEOL, type JFD-9010) onto the fractured surface to obtain a replica film. The replica film was first removed by melting the ice, and then transferred onto a Cu-grid having a 43 μm×43 μm opening. We used a field-emission gun-type TEM (JEOL, type JEM-2010F) to observe the replica film at a 200-kV acceleration voltage. An imaging plate (Fujifilm, type FDL-UR-V) was used for acquiring the observed image.

As found previously [10], MNBs were identified as spherical or oval holes in the replica film. To estimate the size of the MNBs, we measured both the major and minor axes of the hole and calculated the equivalent diameter of a sphere having the same cross-section. We measured at least 40 MNBs for each solution sample to determine an average apparent diameter D. To reduce the observation bias, the data was collected from three replica films made from the same solution. For the measurement of MNB number density N, we counted all MNBs observed in a given grid opening. After averaging the number $\langle n \rangle$ of MNBs in a sample from 5~20 such openings for a replica sample, N was estimated from equation (3) below by assuming a uniform distribution of MNBs in a frozen droplet.

$$N\ [\mathrm{mL}^{-1}] = (\langle n \rangle / 1.85\times10^{-5}\ [\mathrm{cm}^2])^{3/2} \qquad (3)$$

Usually we counted at least 100 MNBs to determine N by adding more than three replica films for each solution sample. The change of D and N were investigated in a time line after the CH_4 hydrate dissociation by repeating the solution sampling.

To compare the MNB distributions from gas hydrate dissociation to a known source of MNB, we prepared MNB-containing water via a commercially supplied MB generator (Aura Tech, type OM4-GP-040). For this reference sample, 500 mL of distilled and deionized water and approximately 0.22 MPa pure CH_4 gas (same sources as for the CH_4 hydrate sample) were mixed in the generator for 1 h at room temperature (approximately 295.2 K). The sampling for the replica preparation was obtained about 1-h after the MNB generation.

Raman spectroscopic measurements were then run on the solution using a Renishaw inVia Reflex micro-

Raman system (250-mm single monochromator) with a 532-nm semiconductor laser. The incident laser beam had a diameter of several tens of micrometers, and a power of about 10 mW. The scattered radiation was collected through a 70-μm slit with 180-degree geometer and dispersed by a 1800-mm^{-1} grating. A CCD detector (1024×256 channels) was used for the Raman signal detection. The Raman spectrum of a silicon wafer (520 cm^{-1}) was used to correct the wavenumber measurement and to estimate the uncertainty of Raman shift as the half-width at half-maximum of the silicon peak, which was approximately 1.1 cm^{-1}. This relatively large uncertainty arises from the system which was set up to obtain the weak Raman spectra from CH_4 molecules in MNBs in the bulk solution. To obtain such signal, a 60-sec exposure spectra was accumulated 5~10 times (which could not be increased due to time constraints for obtaining TEM observation data).

RESULTS AND DISCUSSION

1. Distribution of MNBs in hydrate-dissociated water

TEM images of replica samples indicated that the CH_4 hydrate dissociation produced MNBs in the solution. Several typical examples are shown in Fig. 1. This figure shows holes in the replica with circular or oval-shaped cross-sections of diameter under 1000 nm. As a control, we prepared the freeze-fractured replica sample from distilled and deionized water. We also observed a small amount of MNBs in the control sample. As the water was saturated with air at atmospheric pressure and room temperature, a small amount of air bubbles would be formed when it was rapidly frozen. N in the control sample was the order of 10^7 ml^{-1} in this experiment. Thus we compared the change of N above the order of 10^8 mL^{-1}.

By measuring the apparent size of each hole, we obtained the size distribution of MNBs in a solution. As an example, the solid bar in Fig. 2 shows that the solution three hours after CH_4 hydrate dissociation includes MNB diameters from several tens of nanometers to over 2000 nm with a single maximum at 300–400 nm. For the data in Fig. 2, D = 538 ± 54 nm (the uncertainty shows the standard error). As the fracturing is not controlled, the position of the cross-section should not always pass through the maximum diameters of the bubbles. Thus the estimated D tends to be smaller. However, the TEM–cross-section method nevertheless yields a size distribution nearly the same as that obtained by a dynamic light scattering method [10]. Thus, to qualitatively compare between replica samples after the CH_4 hydrate dissociation this TEM-cross-section

method should be adequate. The method cannot measure MBs exceeding several tens of micrometers because the observable area is limited by the 43-μm-square grid opening. This MNB size distribution is comparable to that prepared with a MB generator (open bar in Fig. 2), which yields to $D = 576 \pm 51$ nm.

We now examine how the storage period after CH_4 hydrate dissociation affects the bubble distribution. Figure 3 shows that the size distribution of MNBs changes gradually during the storage period of the solution. During the dissociation of CH_4 hydrate crystal in water, macroscopic bubbles formed on the crystal surface and disappeared by floating up to the liquid surface. These macroscopic bubbles are too large to be observed by our replica technique. However, the size distributions during and just after hydrate dissociation are nearly the same. This result suggests that macroscopic bubble formation does not change the smaller-sized MNB distribution. The result also suggests that the intense bubble formation and rapid growth of macroscopic bubbles does not affect the smaller-sized MNB size distribution.

After the macroscopic bubbles have fully disappeared, which is about 1-h after complete dissociation, the MNBs smaller than 500-nm in diameter gradually increase in number, with *N* reaching a maximum at 3-h after CH_4 hydrate dissociation. In this condition, both the MNB-size distribution and *D* are similar to those of the MNB-containing water prepared by the MB generator (*N* for thin dashed line in Fig. 3 and *D* for open diamond in Fig. 4), respectively. Therefore, we consider that the MNB obtained by gas hydrate dissociation has a similar distribution to that obtained by the MB generator.

Figures 3 and 4 indicate that *D* and *N* changed synchronously: *D* is smallest at 3-h after dissociation, the time at which *N* is maximum. Then *D* increases during long-term storage of the solution whereas *N* gradually decreases to close to the *N* value for pure water (the control sample). As some MNBs survived in the solution for several days, the solution must be supersaturated, a conclusion supported by a molecular dynamics simulation [23].

After the complete dissociation of the hydrate crystal, the supply of CH_4 molecules into water from the crystal ceased, whereas that from the bubbles remained. As this supply rate decreased, with the large bubbles floating up, and gas being emitted from the open surface of water, the dissolved CH_4 concentration started to decrease. Thus, the number of gas bubbles is expected to decrease with time. However, this study shows that *N* increases for several hours after complete dissociation. *D* decreases simultaneously, so the distribution change of MNBs could be attributed to the shrinkage of large bubbles. These processes are expected to be common during the formation of artificial MNBs [4].The fact that some MNBs remain in the solution several

days after dissociation suggests 1) that the rate of bubble rise is sufficiently small and 2) that the CH_4 concentration surrounding the MNBs remains sufficiently high. However, the gradual decrease in the CH_4 concentration in the solution results in a decrease of N.

The MNB may aid the memory effect of gas hydrate reformation [18, 19]. The CH_4 molecules (as well as most other hydrate guest molecules) have a low solubility in water due to their hydrophobicity. Thus, long-lived MNBs would effectively work as a storage medium for guest molecules in the water. If the pressure and temperature conditions of the solution return to those of CH_4 hydrate stability, these MNBs would then become the source of hydrate guest molecules, thus stimulating more rapid nucleation than that of the initial nucleation, which involves a supply of guest molecule only from the surface of water.

2. Measurements of MNB solutions via Raman spectroscopy

Although we observed MNBs in the replica film, the image does not identify them as CH_4 MNBs. Thus we ran Raman spectroscopic measurements on the CH_4-hydrate dissociated solutions to confirm whether bubbles contain CH_4. This measurement also allows us to estimate P_g of the CH_4 MNB experimentally. P_g is usually estimated from eq. (2) by assuming a simplified system with assumed conditions. By measuring P_g in the CH_4 MNB, we can estimate the CH_4 content in the bubble and consider the mass balance of CH_4 in the solution. This mass balance allows us to examine how MNBs contribute to the memory effect on gas hydrate reformation.

During and just after the CH_4 hydrate dissociation, macroscopic bubbles frequently formed. Under this condition, we obtained the single peak of the ν_1 mode at 2917.6 cm^{-1} (Fig. 5a, dotted line), which indicates the existence of CH_4 vapor at atmospheric pressure [24]. Simultaneously, we find CH_4 peaks in the hydrate phase during the dissociation at 2903.8 and 2915.3 cm^{-1} (Fig. 5a, solid line), which are consistent with previously reported data [25, 27].

After the complete dissociation of the bulk hydrate crystal, these strong spectra of CH_4 molecules could not be detected in the bulk liquid. To obtain a Raman peak from MNBs in such solution, we accumulated longer-exposure measurements. As the tail of the O-H stretching peak of water (observed mainly at 3000~3800 cm^{-1}) overlaps the baseline of this region, we subtracted the baseline by assuming that the tail of the O-H stretching peak is parabolic. As a result, a small peak emerges at 2916.2 ± 1.1 cm^{-1} (Fig. 5b; thick solid line, marked by an open arrow). This peak is neither the atmospheric CH_4 peak nor the dissolved CH_4

peak (2910 cm^{-1} [28]), but exists in the C-H stretching mode of CH_4 vapor under high pressure [24]. Therefore, we assigned the 2916.2 cm^{-1} peak to the ν_1 mode of CH_4 molecule in MNBs in bulk water. The reproducibility of this peak was checked three times in different sample sets.

Based on the peak-shift data of the ν_1 mode under various pressures [24], this Raman peak indicates that the CH_4 molecules are in a vapor at about 7 ± 5 MPa. Although the estimate of P_g has a large uncertainty, this is the first direct measurement of P_g in MNBs. This value is smaller than the dissociation pressure P_d = 21.3 MPa for CH_4 hydrate at about 292 K [18]. As the released CH_4 molecules are dissolved into water prior to the bubble formation when CH_4 hydrate is dissociating in water, as shown experimentally [29] and theoretically [20-23], it is reasonable that P_g in CH_4 MNB should be less than P_d.

The Raman spectra measurement on CH_4-hydrate dissociated solution was previously reported under high pressure condition [28]. Then we compare our results with the previous data with some reanalyses. When CH_4 hydrate crystals were dissociated under high pressure condition (P_l = 10 MPa and 286 K), the weak C-H stretching mode Raman spectra were obtained in the aqueous phase about 10-mm away from the edge of the solid phase. By averaging the spectra in the aqueous phase, from 8 to 18 mm from the edge, we identified three peaks: two CH_4 peaks in large and small cages (2904.5 and 2914.1 cm^{-1}) and one dissolved CH_4 peak (2909.3 cm^{-1}). Since the dissolved CH_4 peak position is independent of pressure up to 20 MPa (reanalyzed data in [28]), the cage-like structures have been considered to be able to survive in the CH_4-saturated solution under high pressure. If the CH_4 MNBs co-existed in that system, however, the CH_4 peak in MNBs would overlap at 2914.1 cm^{-1}. At that wavenumber, P_g is estimated to be approximately 16 MPa. This value is 6 MPa higher than P_l at that condition, so the pressure difference is comparable with that obtained in the present study. Therefore, it is possible that both cage-like structures associated with CH_4 molecules and CH_4 MNBs coexisted in the CH_4-hydrate dissociated solution under high pressure. In the present study, on the other hand, we could obtain neither CH_4 spectra included in cages nor dissolved in the solution under atmospheric pressure (Fig. 5b). Thus we consider that the CH_4 hydrate crystal dissociates completely under atmospheric pressure and forms MNBs only in the solution after saturating with CH_4.

As a simple estimate, consider that all MNBs have the average diameter of about 600 nm with P_g. Assuming the density difference of CH_4 under P_g = 7 MPa and atmosphere pressure [30], this pressure would be obtained when a bubble of 2.6-μm diameter at atmospheric pressure contracts to 600 nm. This size of about 2.6 μm was identified in the solution during and just after the CH_4 hydrates dissociation (Fig. 3). Thus,

the MNB formation can be interpreted not only by the aggregation of CH_4 molecules dissolved in water [20-23], but also by the shrinkage of larger bubbles formed during the hydrate dissociation.

In contrast, we can estimate the apparent size of CH_4 MNBs from P_g with the Young-Laplace equation (eq. (2)). When we assume σ to be about 63 mN m^{-1} at 7 MPa (from [31]), a bubble with P_g = 7 ± 5 MPa would have the diameter from 19 to 126 nm. This is smaller than the average diameter obtained in the present study. The discrepancy may be mainly due to a large uncertainty in the estimate of P_g of MNBs via Raman spectroscopy and that of D via TEM observation. However, if our estimation is available, some assumptions in eq. (2), such as setting σ to be the value in bulk system, should require some modifications in the practical system.

Now we consider the material balance of CH_4 molecules in the CH_4 hydrate dissociation process. CH_4 molecules in water are either in solute or in MNBs, all of which are assumed to be originally came from the CH_4 hydrate crystal (5×10^{-3} mol mL^{-1}, assuming a cage occupancy of 0.93 [25] and a hydrate fraction in the sample of 0.7). The solubility of CH_4 in water at 293.2 K is 3.3 mL/100 mL-water (or 1.4×10^{-6} mol mL^{-1}-water [32]). On the other hand, CH_4 molecules in MNBs of concentration 2×10^{9} mL^{-1}, each having 600-nm diameter with P_g = 7 MPa, gives a total of about 6.5×10^{-7} mol mL^{-1}-water. This value is almost a half of those in the saturated solution. The total CH_4 molecules in the CH_4-hydrate dissociated solution are then only 300 ppm of the source in the CH_4-hydrate crystal. The most of the residual CH_4 molecules would have been released from the liquid phase to the vapor as the macroscopic bubbles and MBs observed during and just after the CH_4 hydrate dissociation. Although this total value of CH_4 molecules in the dissociated solution seems to be small, one half of the CH_4 molecules existed in water concentrated in MNBs, which existed in a certain location near the solid hydrate was existed for a period as long as the memory effect is expressed. As such, MNBs can have an important role in the memory effect of CH_4 hydrate reformation.

Sloan and Koh [18] summarized several features of the memory effect. These features may be explained by the behavior of MNBs. For example, the memory effect vanishes when the dissolved solution is heated up to 301.2 K. As the heating would decrease the solubility of CH_4 in water, it would inhibit the memory effect by the MNB disappearance. The memory effect also vanishes after long-term storage. This effect would also result from the gradual disappearance of MNBs, as shown in Fig. 3. This disappearance may have resulted from the MNBs floating up to the surface or dissolving into water due to the CH_4 concentration in the solution becoming undersaturated.

Other processes involving water structurization may also contribute to the memory effect (the first hypothesis). Our results allow these possibilities. Since guest molecules are usually hydrophobic, the water surrounding the MNB would be highly hydrogen bonded as predicted by Ohgaki et al. [9]. Although there is no evidence that this structure is clathrate-like, a structured water network could be a trigger of the hydrate nucleation. Even in this process, the concentration of guest molecules is crucial, which suggests the existence of MNBs in the solution.

CONCLUSION

The formation of micro- and nano-bubbles (MNBs) after CH_4 hydrate dissociation in water was identified using transmission electron microscopic observations of freeze-fracture replicas. The distributions of the MNBs stabilized within several hours after dissociation, reaching an average diameter of about 600 nm and a number concentration of order 10^9 mL^{-1}. These values are consistent with those obtained using a commercially supplied microbubble generator. Thus, we conclude that gas hydrate dissociation is a simple and effective method to obtain MNB solution.

Applying Raman spectroscopy to the CH_4-hydrate-dissociated water allowed us to confirm that the MNB contained CH_4 vapor at high pressure. The red shift of the ν_1 mode peak of CH_4 molecules indicated an internal pressure of MNBs of 7 ± 5 MPa. Based on these results, we argued that MNBs produce a memory effect on hydrate recrystallization. In particular, the MNBs formed after the dissociation would act as a storage material for guest molecules in water.

ACKNOWLEDGEMENTS

This work was partly supported financially by a Grant-in-Aid for Scientific Research from the Japan Society for the Promotion of Science (Grant Nos. 23350001 and 25600035). Raman spectroscopic measurements were performed with Renishaw inVia Reflex micro-Raman system at the OPEN FACILITY, Hokkaido University Sousei Hall. FEG-TEM observations were financially supported by the Nanotechnology Platform program and technically supported by Dr. N. Sakaguchi (Hokkaido Univ.).

REFERENCES

1. S. Oshita, T. Uchida, Basic Characterization of Nanobubbles and Their Potential Application, in "Bio-Nanotechnology: A Revolution in Biomedical Sciences, & Human Health (Eds. by D. Bagchi, M. Bagchi, H. Moriyama, F. Shahidi)", Chap 29, John Wiley & Sons, Ltd., 506-516 (2013).

2. H. Tsuge, The latest technology on microbubbles and nanobubbles (in Japanese), in Maikurobaburu no tokusei (Special characteristics of microbubbles), Chap. 2, Tokyo: CMC, 15-30 (2007).

3. R. Clift, J.R. Grace, M.E. Weber, Bubbles, Drops and Particles, Mineola: Dover Pub, (2005).

4. F.Y. Ushikubo, Fundamental studies on the state of water with the generation of micro and nano-bubbles (PhD thesis), Univ Tokyo, (2010).

5. S. Ljunggren, J.C. Eriksson, The lifetime of a colloid-sized gas bubble in water and the cause of hydrophobic attraction, *Colloids Surf. A Physicochem. Eng. Aspects*, **129-130**, 151-155 (1997).

6. M. Takahashi, Application to the agricultural and food fields of the microbubbles and nanobubbles (in Japanese), *Food Technology (FOO-TECH) Forum, 2006 Japanese Society of Agricultural Machinery (JSAM) Symposium*, 24-31 (2006).

7. M. Switkes, J.W. Ruberti, Rapid cryofixation/freeze fracture for the study of nanobubbles at solid-liquid interfaces, *Appl. Phys. Lett.*, **48**, 4759-4761 (2004).

8. E. Dressaire, R. Bee, A. Lips, H.A. Stone, Interfacial polygonal nanopatterning of stable microbubbles, *Science*, **320**, 1198-1201 (2008).

9. K. Ohgaki, N.Q. Khanh, Y. Joden, A. Tsuji, T. Nakagawa, Physicochemical approach to nanobubble solutions, *Chem. Eng. Sci.*, **65**, 1296-1300 (2010).

10. T. Uchida, S. Oshita, M. Ohmori, T. Tsuno, K. Soejima, S. Shinozaki, Y. Take, K. Misuda, Transmission electron microscopic observations of nanobubbles and their capture of impurities in wastewater, *Nanoscale Res. Lett.*, **6**, 295 (2011).

11. S. Liu, S. Oshita, Y. Makino, Q. Wang, Y. Kawagoe, T. Uchida, Oxidative capacity of nanobubbles and its effect on seed germination, *ACS Sustainable Chemistry & Engineering*, in press.

12. E.D. Sloan, Jr., Hydrate Engineering, SPE monograph 21, Richardson, TX: SPE Inc, (2000).

13. H. Mimachi, S. Takeya, A. Yoneyama, K. Hyodo, T. Takeda, Y. Gotoh, T. Murayama, Natural gas storage and transportation within gas hydrate of smaller particle: Size dependence of self-preservation phenomenon

of natural gas hydrate, *Chem. Eng. Sci.* **118**, 208-213 (2014).

14. M. Kurihara, A. Sato, H. Ouchi, H. Narita, Y. Masuda, T. Saeki, T. Fujii, Prediction of Gas Productivity From Eastern Nankai Trough Methane-Hydrate Reservoirs, *SPE Reservoir Evaluation Eng.*, **12**, 477-499 (2009).

15. Y. Masuda, S. Nagakubo, M. Satoh, T. Uchida, Methane Hydrates, in World Scientific Handbook of Energy, Chapter 10, World Scientific Pub Co, in press.

16. J.S. Parent, P.R. Bishnoi, Investigations into the Nucleation Behavior of Methane Gas Hydrates, *Chem. Eng. Commun.* **144**, 51-64 (1996).

17. S. Takeya, A. Hori, T. Hondoh, T. Uchida, Freezing-memory effect of water on nucleation of CO_2 hydrate crystals, *J. Phys. Chem. B*, **104**, 4164-4168 (2000).

18. E.D. Sloan, C.A. Koh, Clathrate Hydrate of Natural Gases, 3rd edition, Boca Raton, FL: CRC Press, (2007).

19. P.M. Rodger, Methane Hydrate Melting and Memory, *Ann. N.Y. Acad. Sci.*, **912**, 474-482 (2000).

20. S.A. Bagherzadeh, P. Englezos, S. Alavi, J.A. Ripmeester, Molecular simulation of non-equilibrium methane hydrate decomposition process, *J. Chem. Thermodynam.*, **44**, 13-19 (2012).

21. S.A. Bagherzadeh, S. Alavi, J.A. Ripmeester, P. Englezos, Evolution of methane during gas hydrae dissociation, Fluid Phase Equilibria, **358**, 114-120 (2013).

22. S.A. Bagherzadeh, S. Alavi, J.A. Ripmeester, P. Englezos, Formation of methane nano-bubhles during hydrate decomposition and their effect on hydrate growth, *J. Chem. Phys.*, **142**, 214701-1-8 (2015).

23. T. Yagasaki M. Matsumoto Y. Andoh S. Okazaki H. Tanaka, Effect of bubble formation on the dissociation of methane hydrate in water: A molecular dynamics study, *J. Phys. Chem. B*, **118**, 1900-1906 (2014).

24. F. Lin, A.K. Sum, R.J. Bodnar, Correlation of methane Raman ν_1 band position with fluid density and iteractions at the molecular level, *J. Raman Spectrosc.*, **38**, 1510-1515 (2007).

25. T. Uchida, T. Hirano, T. Ebinuma, H. Narita, K. Gohara, S. Mae, R. Matsumoto, Raman spectroscopic determination of hydration number of methane hydrates, *AIChE J.*, **45**, 2641-2645 (1999).

26. T. Uchida, M. Nagayama, T. Shibayama, K. Gohara, Morphological investigations of desaccharide molecules for growth inhibiton of ice crystals, *J. Crystal Growth*, **299**, 125-135 (2007).

27. A.K. Sum, R.C. Burruss, E.D. Sloan, Jr, Measurement of clathrate hydrates via Raman spectroscopy, *J.*

Phys. Chem. B, **101**, 7371–7377 (1997).

28. T. Uchida, R. Okabe, K. Gohara, S. Mae, Y. Seo, H. Lee, S. Takeya, J. Nagao, T. Ebinuma, H. Narita, Raman spectroscopic observations of methane-hydrate formation and hydrophobic hydration around methane molecules in solution, *Can. J. Phys.*, **81**, 359-366 (2003).

29. D. Katsuki, R. Ohmura, T. Ebinuma, H. Narita, Visual observation of dissociation of methane hydrate crystals in a glass micro model: Production and transfer of methane, *J. Appl. Phys.*, **104**, 083514 (2008).

30. JSME Data book: Thermophysical Properties of Fluids, *Jpn. Soc. Mech. Engrs.*, Tokyo, Japan, 255 (1983).

31. S. Khosharay, F. Varaminian, Experimental and modeling investigation on surface tension and surface properties of (CH_4+H_2O), (C_2H_6+H_2O), (CO_2+H_2O) and (C_3H_8+H_2O) from 284.15 K to 312.15 K and pressures up to 60 bar, *Int. J. Refrigeration*, **47**, 26-35 (2014).

32. International Chemical Safety Cards ICSC0291.

Figure captions

Figure 1. TEM images of micro- and nano-bubbles (MNBs) in the replica after CH_4 hydrate dissociation. (a, b) One hour after dissociation. (c, d) Three hours after dissociation. Each scale bar shows 500 nm.

Figure 2. MNB size distributions. Solid bar: 3 hours after CH_4 hydrate dissociation (n = 105); open bar: obtained by the MB generator (n = 182). Frequency is standardized by n. For oval shapes, diameter is average of major and minor widths.

Figure 3. Cumulative distribution of MNB diameter *vs* number concentration.
Dotted line: during dissociation; dashed line: 15-min after dissociation; thin solid line: 1-hour after dissociation; thick solid line: 3-hours after dissociation; gray solid line: 3-days after dissociation; dot-and-dash line: 4-days after dissociation; and thin dashed line: MNB-containing water

Figure 4. Average diameter of MNBs in solution *vs* storage period.
Solid circle: MNBs from CH_4 hydrate dissociation; open diamond: MNBs prepared by the MB generator. Error bars show the standard deviation of the average diameter in each replica sample.

Figure 5. Raman spectra of CH_4 ν_1 mode. (a) From a CH_4 hydrate crystal (solid line) and in CH_4 vapor at atmospheric pressure (dotted line). (b) From MNBs formed by gas hydrate dissociation (solid line). The peak marked by an arrow is likely from CH_4 vapor in the MNBs.

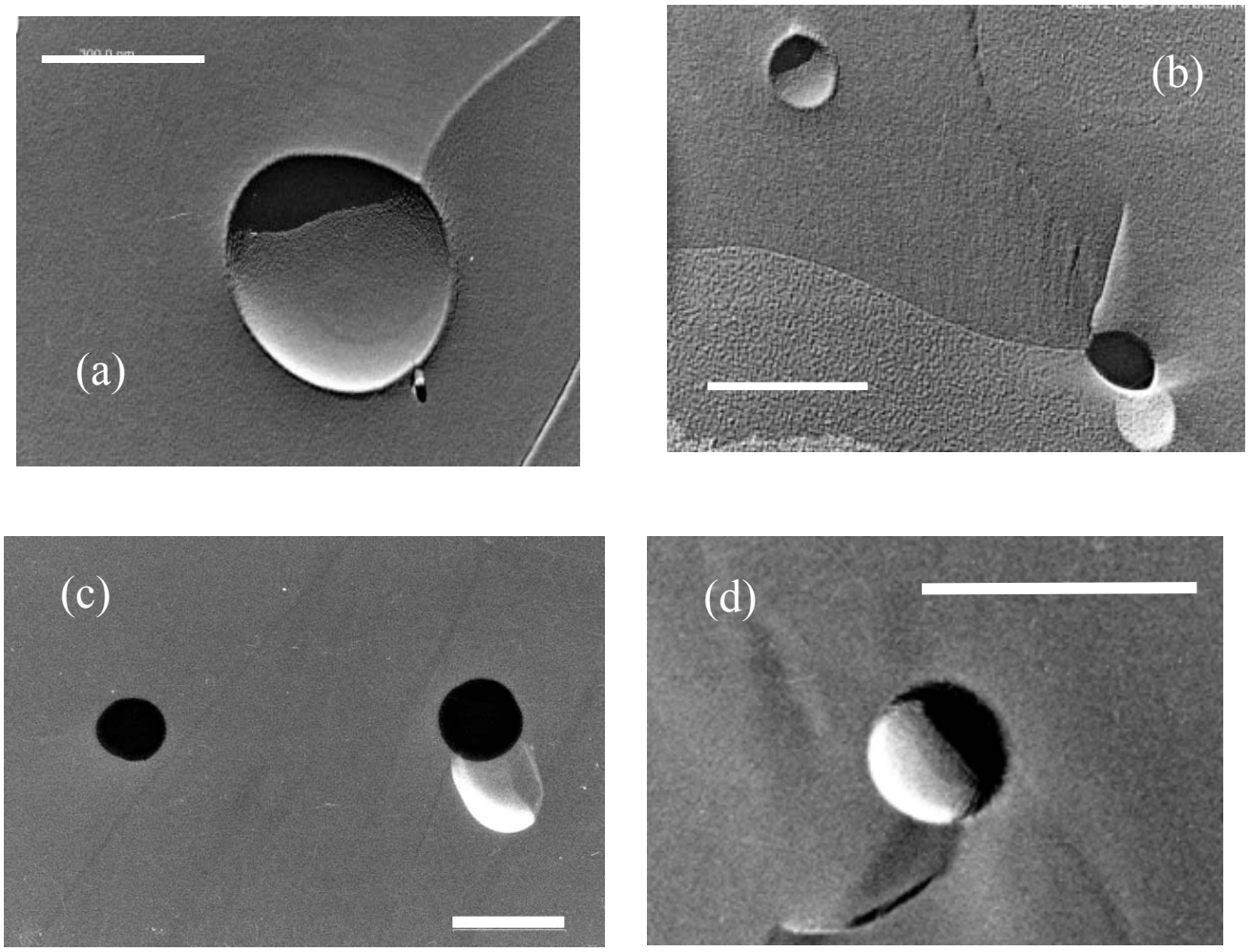

Figure 1. TEM images of micro- and nano-bubbles (MNBs) in the replica after CH_4 hydrate dissociation. (a, b) One hour after dissociation. (c, d) Three hours after dissociation. Each scale bar shows 500 nm.

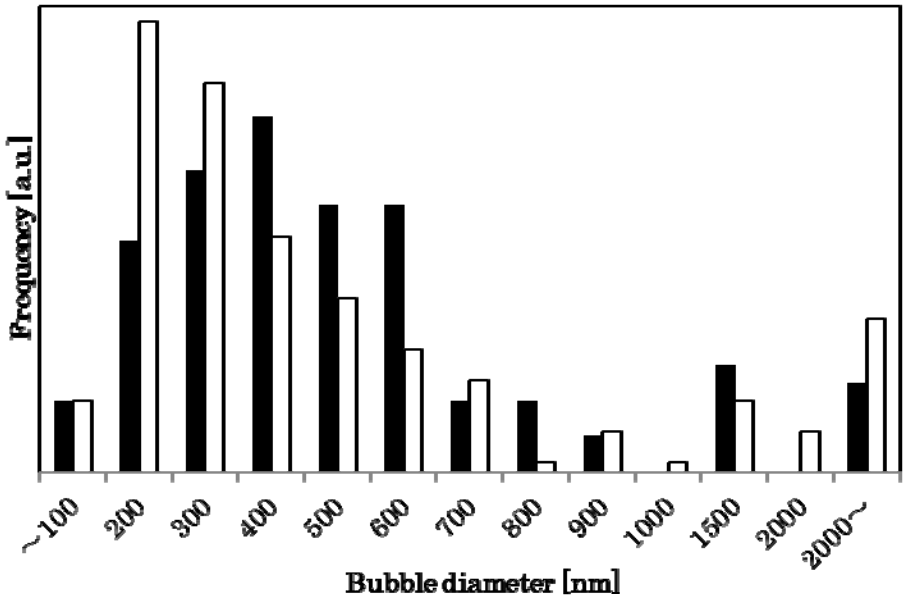

Figure 2. MNB size distributions.

Solid bar: 3 hours after CH_4 hydrate dissociation (n = 105); open bar: obtained by the MB generator (n = 182). Frequency is standardized by n. For oval shapes, diameter is average of major and minor widths.

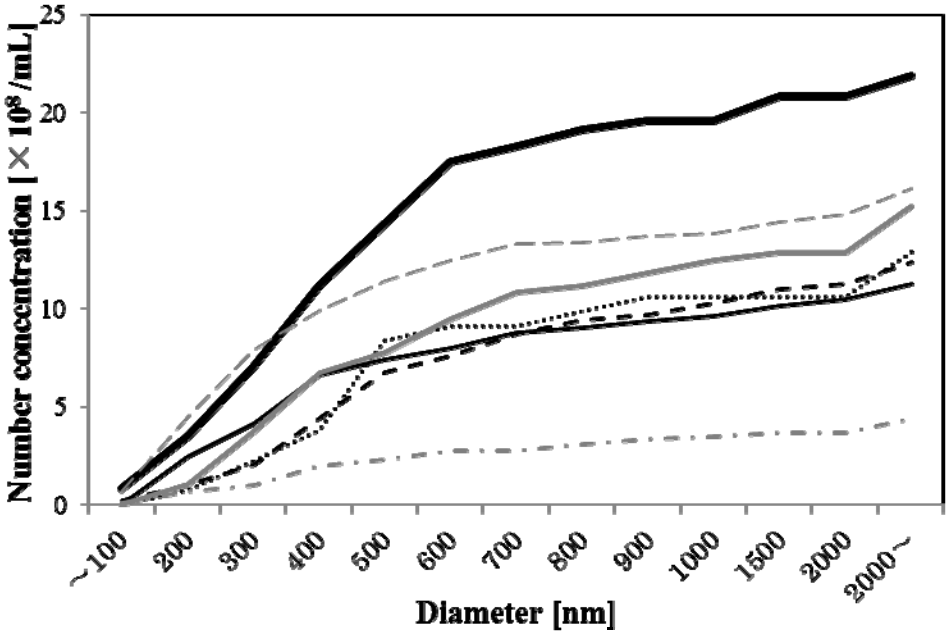

Figure 3. Cumulative distribution of MNB diameter *vs* number concentration.

Dotted line: during dissociation; dashed line: 15-min after dissociation; thin solid line: 1-hour after dissociation; thick solid line: 3-hours after dissociation; gray solid line: 3-days after dissociation; dot-and-dash line: 4-days after dissociation; and thin dashed line: MNB-containing water

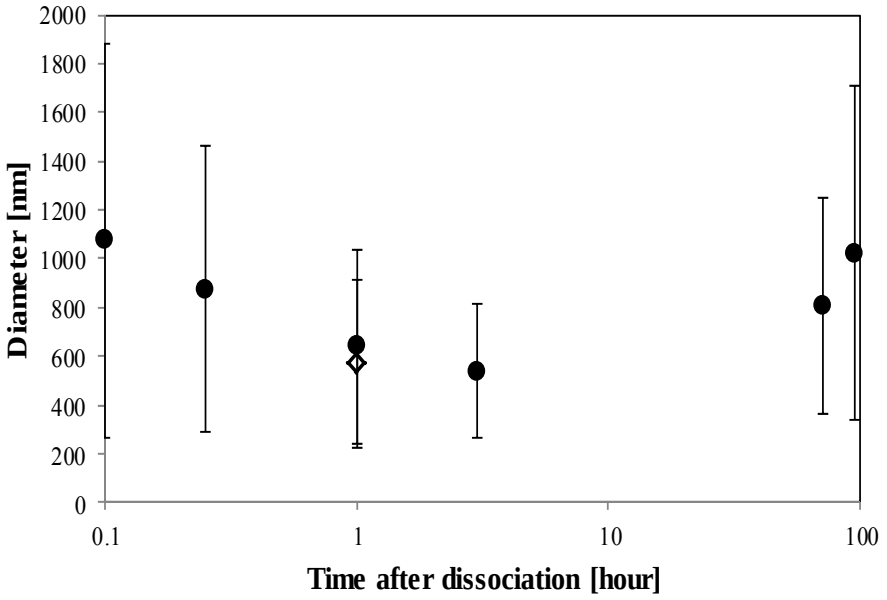

Figure 4. Average diameter of MNBs in solution *vs* storage period.

Solid circle: MNBs from CH_4 hydrate dissociation; open diamond: MNBs prepared by the MB generator. Error bars show the standard deviation of the average diameter in each replica sample.

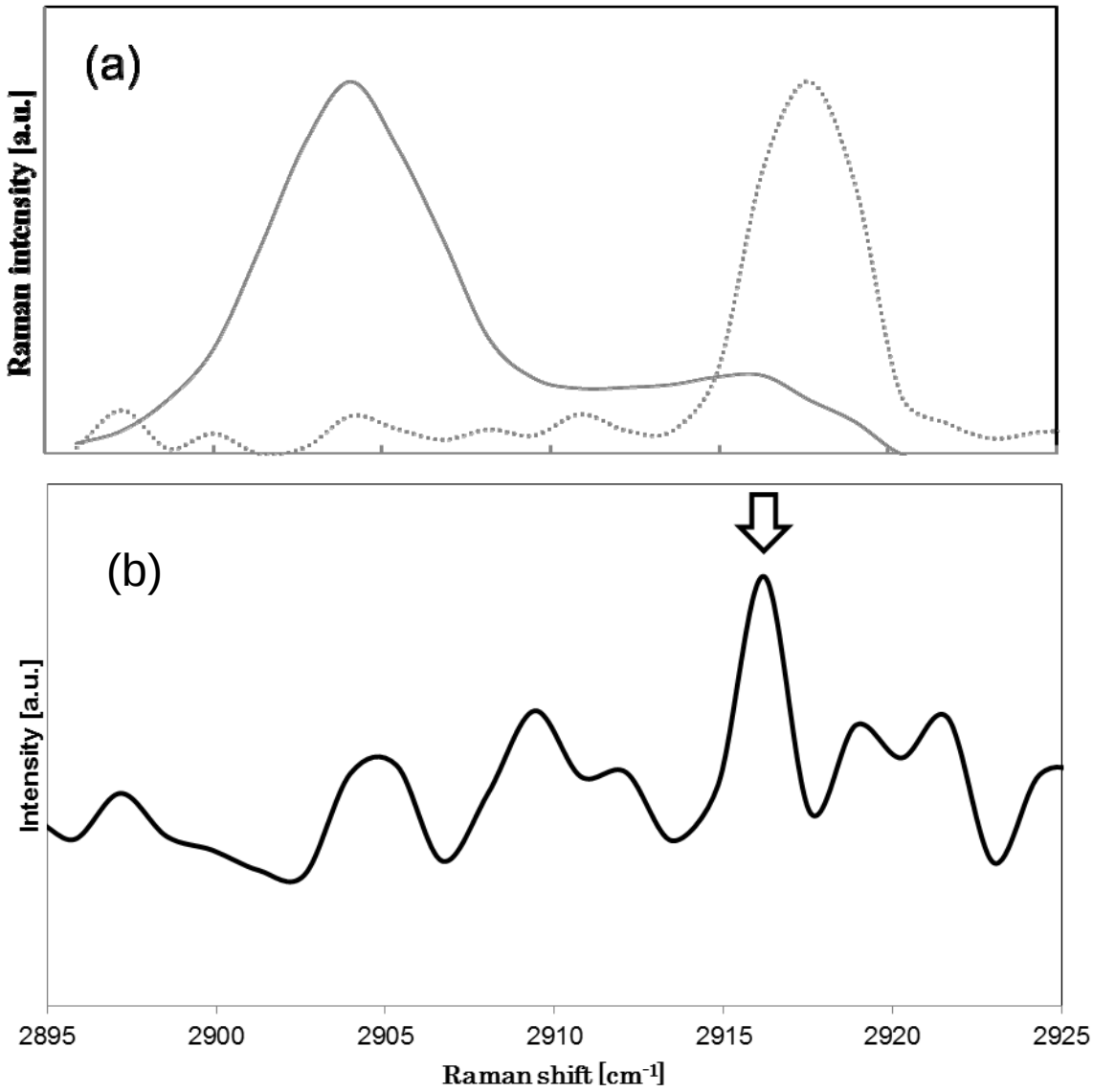

Figure 5. Raman spectra of CH_4 ν_1 mode.

(a) From a CH_4 hydrate crystal (solid line) and in CH_4 vapor at atmospheric pressure (dotted line).

(b) From MNBs formed by gas hydrate dissociation (solid line). The peak marked by an arrow is likely from CH_4 vapor in the MNBs.